JANUARY 1977 PPPL-1315

RADIAL BOUNDARY LAYERS IN DIFFUSING TOROIDAL EQUILIBRIA

BY

M. D. ROSEN AND J. M. GREENE

PLASMA PHYSICS LABORATORY

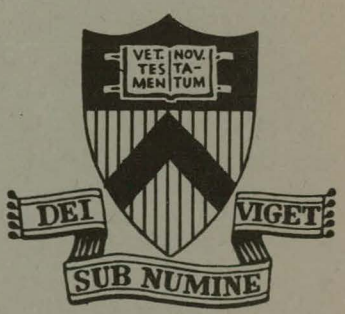

*

PRINCETON UNIVERSITY
PRINCETON, NEW JERSEY

This work was supported by U. S. Energy Research and Development Administration Contract E(11-1)-3073. Reproduction, translation, publication, use and disposal, in whole or in part, by or for the United States Government is permitted.

DISCLAIMER

NOTICE

Printed in the United States of America.

Available from
National Technical Information Service
U. S. Department of Commerce
5285 Port Royal Road
Springfield, Virginia 22151
Price: Printed Copy $ * ; Microfiche $3.00

*Pages	NTIS Selling Price
1-50	$ 4.00
51-150	5.45
151-325	7.60
326-500	10.60
501-1000	13.60

Radial Boundary Layers in Diffusing Toroidal Equilibria

M. D. Rosen and J. M. Greene

Plasma Physics Laboratory, Princeton University
Princeton, New Jersey 08540

PPPL-1315

January 1977

Radial Boundary Layers in Diffusing Toroidal Equilibria

M. D. Rosen* and J. M. Greene

Plasma Physics Laboratory, Princeton University

Princeton, New Jersey 08540

ABSTRACT

Analytic results in straight cylindrical geometry imply sharp density gradients near the boundary of a plasma decaying by classical diffusion. Utilizing an isothermal one-fluid magnetohydrodynamic model, we apply these results to toroidal configurations and obtain a set of nonlinear equations for a radial boundary layer. A dominant effect in this regime is convective plasma flow along magnetic lines of force, with velocity in the sonic range. This flow pattern matches onto the interior solution of Pfirsch-Schlüter convective flow. Solutions separable in the radial and poloidal directions are found that fulfill both boundary and periodicity conditions, and that result in both smooth subsonic poloidal flow, and weak shock transonic flows. Effects of the flow patterns on diffusion are discussed.

I. INTRODUCTION

Most studies of toroidal plasma confinement have been characterized by the assumption that the plasma is in static equilibrium. However, about six years ago many papers appeared in the literature that studied inertial (and dissipative) effects in toroidal systems. Poloidal rotations, weak shocks, and enhanced diffusion due to flows were among the main topics under investigation. An excellent review paper by Green[1] contains over fifty references on these subjects.

In this paper, we take a critical look at some of those papers,[2] with special emphasis on fulfilling boundary conditions at a perfectly conducting material limiter and particularly on the plasma behavior in a region near that limiter. We find a condition on the steepening of the density gradient near the limiter by studying a plasma diffusing classically in a straight system. This condition is applied, in leading order, to a toroidal system and is found to cause a breakdown of the usual expansion in inverse aspect ratio. This results in a radial boundary layer near the plasma edge, the solution of which is the main objective of this paper.

In order to understand the appearance of radial boundary layers and the meaning of their velocity flow patterns, we must first fully understand the bulk plasma solution. In the bulk plasma region, density gradients are mild, $(d\rho/dr) \sim \rho/a$, as opposed to the boundary layer region near the edge where ρ is small and which will be shown to behave as $(d\rho/dr) \sim 1/\rho$.

This bulk plasma region has been investigated extensively, and demonstrates Pfirsch-Schlüter current and velocity convection patterns, shown in Fig. 1. The physical mechanisms behind this flow pattern are due mainly to the 1/R behavior of the toroidal field, and to resistivity. Ions drift upward and electrons downward in this toroidal field. The rotational transform (poloidal field) permits rapid neutralization of the resultant $\vec{E}$ field caused by the charge separation. However, in a resistive plasma, this neutralization is incomplete. Consider the remaining un-neutralized groups of ions and electrons localized at the upper and lower flow stagnation points of Fig. 1a. These produce a static $\vec{E}$ field that yields the $\vec{E} \times \vec{B}$ drift flow pattern of Fig. 1a. This, in turn, causes a pressure imbalance along field lines that is neutralized by flows parallel to the field lines. The poloidal and toroidal components of this flow are shown in Figs. 1a and 1c. Plasma inertia prevents complete neutralization of the pressure, so that pressure gradients remain along field lines.

Near the plasma boundary, density gradients, electric fields, and flow velocities become increasingly large. When the poloidal velocity approaches the reduced sound speed, pressure variations over a magnetic surface become finite. At the reduced sound speed, transonic flow and shocks come into existence. These effects, in the boundary layer, are the subject of this paper.

The model used is described in Sec. II. In Sec. III, we consider a straight cylindrical configuration and solutions to the diffusion equation in

such a system. A resulting steep density gradient condition, near the plasma edge, is applied to a toroidal system in Sec. IV. The boundary layer equations are derived, and separable solutions in the radial and poloidal directions are found. In Sec. V, we discuss subsonic, smoothly flowing, poloidal behavior in the boundary layer, while in Sec. VI we find different solutions of a transonic and weak shock nature. Section VII concludes the analysis with a look at the effects of these flow solutions on the diffusion. Section VIII contains conclusions and some remarks on the assumptions of the model.

II. MODEL

We consider the following fluid model for a plasma in a highly collisional regime. The pressure is a scalar, and we further simplify the model by making an isothermal approximation. With s denoting the sound speed, ρ the density, and η a scalar resistivity, our one-fluid magnetohydrodynamic model becomes

$$\rho \frac{\partial \vec{v}}{\partial t} + \vec{v} \cdot \vec{\nabla} \vec{v} = \frac{1}{c} (\vec{j} \times \vec{B}) - s^2 \vec{\nabla} \rho , \tag{1}$$

$$\vec{\nabla} \phi = \frac{1}{c} (\vec{v} \times \vec{B}) - \eta \vec{j} , \tag{2}$$

$$\frac{\partial \rho}{\partial t} + \vec{\nabla} \cdot (\rho \vec{v}) = 0 , \tag{3}$$

$$\vec{\nabla} \cdot \vec{J} = 0 . \tag{4}$$

We have kept the inertia terms in the force law, and have assumed a low β $[(P/B^2) \ll 1]$, which makes perturbations of the magnetic field

associated with mass diffusion negligibly small. As such, the magnetic field is static and allows $\vec{E} = -\vec{\nabla}\phi$ in Ohm's law. In addition, Ampere's law is replaced by charge conservation Eq. (4). A final consequence of the low-β approximation is the "Knorr Model"[4] magnetic field. In the usual toroidal system, Fig. 2, the magnetic field lines form concentric surfaces of radius r; θ is an angle around the magnetic axis, and z is measured along this axis. We represent the magnetic field as

$$\vec{B} = (B_o/N)[f(r)\,\hat{e}_\theta + \hat{e}_z] \quad , \tag{5}$$

with

$$N \equiv 1 - (r/R)\cos\theta \tag{6}$$

and $f(r)$ representative of the poloidal field.

Since the fluid equations have a preferred direction along the field lines, it is convenient to decompose vectors as

$$\vec{v} \equiv v_r \hat{e}_r + v_s B_o[(\vec{B}\times\hat{e}_r)/B^2] + v_b B_o(\vec{B}/B^2) \tag{7}$$

$$= v_r \hat{e}_r + [N/(1+f^2)][(v_s + fv_b)\,\hat{e}_\theta + (v_b - fv_s)\,\hat{e}_z] \quad . \tag{8}$$

To help in the solution of our basic set [Eqs. (1) - (4)], we adopt an optimal ordering designed to include as much relevant physics as possible[2]

$$\frac{a}{\epsilon R} \sim \frac{f}{\epsilon} \sim \frac{v_b}{s} \sim \frac{v_s}{\epsilon s} \sim \frac{v_r}{\epsilon^2 s} \sim \frac{\partial/\partial t}{\epsilon^3} \sim \frac{\eta}{\epsilon^3} \sim 1 \quad . \tag{9}$$

Note that we are considering a slowly evolving equilibrium decaying by means of classical diffusion on a $(\partial/\partial t) \sim \eta \sim \epsilon^3$ time scale.

III. STRAIGHT SYSTEM

Before studying our large aspect ratio toroidal system we consider a straight cylindrical configuration. This will provide a guideline for choosing a density profile for the toroidal case. The justification for this approach is that in toroidal geometry we expand in $\epsilon \equiv a/R$. The density ρ can then be expressed as

$$\rho = \rho^{(0)}(r) + \rho^{(1)}(r,\theta) + \ldots \quad ,$$

where $\rho^{(0)}(r)$ is an arbitrary function. Thus the leading order $\rho^{0}(r)$ should be determined from the straight system and then applied to toroidal geometry. The existence of Pfirsch-Schlüter terms in the diffusion makes this statement only qualitatively correct, but that is all that is needed here.

In the straight system, Eq. (3) becomes

$$\frac{\partial \rho}{\partial t} + \frac{1}{r}\frac{\partial}{\partial r}(r\rho v_r) = 0 \quad . \tag{10}$$

From the radial component of the force law we obtain

$$J_s = (cs^2/B_o)(\partial\rho/\partial r) \quad , \tag{11}$$

and from $\vec{B} \times (\text{Ohm's law})\cdot\hat{e}_r$, we obtain

$$v_r = -(\eta c/B_o) j_s \quad , \tag{12}$$

Therefore, Eq. (10) becomes

$$\frac{\partial \rho}{\partial t} = \frac{1}{r}\frac{\partial}{\partial r}\left(\frac{r\eta c^2 s^2}{B^2}\frac{\rho\,\partial\rho}{\partial r}\right) \quad . \tag{13}$$

This has the similarity solution[5]

$$\rho = X(r)\rho_o \left[1 + (\eta c^2 s^2 \rho_o \lambda t / B_o^2 a^2)\right]^{-1} \quad , \tag{14}$$

and thus reduces Eq. (13) to an eigenvalue equation

$$-\lambda X = \frac{a^2}{r} \frac{d}{dr} \left(r X \frac{dX}{dr} \right) \quad . \tag{15}$$

This equation has been solved numerically[6] subject to the boundary conditions $(dX/dr) = 0$ at $r = 0$, and $X = 0$ at $r = a$. (A limiter absorbs all particles that venture past $r = a$.) The solution is $\lambda = 2.28$, and is shown in Fig. 3a.

Near $r = a$, the density is small, and Eq. (15) yields

$$\left[\frac{1}{a} \frac{d}{dr} \left(aX \frac{dX}{dr} \right) \right] = 0 \quad , \tag{16}$$

or equivalently

$$(d\rho/dr) \sim (1/\rho) \quad , \tag{17}$$

so that the density gradients are large. This density gradient steepening behavior is the key to the toroidal boundary layers that will follow in the next section.

If instead of a diffusing equilibrium we studied[7] one maintained by a plasma source $Q(r)$,

$$\frac{1}{r} \frac{\partial}{\partial r} (r \rho v_r) = Q(r) \quad , \tag{18}$$

we can also find conditions on $\rho(r)$ near $r = a$, Fig. 3a could just as well

be the solution of Eq. (18) for a constant source $Q(r) = 2\,q_0$, while Fig. 3b describes the solution for $Q(r) = 4\,q_2 r^2$, representing a more realistic distribution of neutrals as a plasma source, as they are more numerous near the plasma edge. Nonetheless, either source yields a $\rho(r)$ such that, near $r = a$, the steepness condition, Eq. (17), still holds.

IV. TOROIDAL SYSTEM AND BOUNDARY LAYER

As described in the introduction, the bulk plasma behavior in a toroidal system has a characteristic convective flow pattern (Fig. 1). Near the plasma edge the density gradients and flows will become large and a boundary layer will be needed to describe this region. For the bulk plasma solution, we find,[2] expanding in powers of ϵ, that $\rho = \rho^{(0)}(r) + \rho^{(1)}(r,\theta)$, where

$$\rho^{(1)}(r,\theta) \sim \epsilon\,(d\rho^{(0)}/dr)^2 \sin\theta \ .$$

This is fine as long as $(d\rho^{(0)}/dr) \sim \rho^0/a \sim \epsilon^0$. However, near the plasma edge Eq. (17) holds, $(d\rho^{(0)}/dr) \sim (1/\rho^{(0)})$, so a breakdown will occur when $\rho^{(0)}$ drops to order $\epsilon^{1/3}$. Then $\rho^{(1)} \sim \epsilon\,(1/\epsilon^{1/3})^2 \sim \epsilon^{1/3} \sim \rho^{(0)}$. To be consistent with Eq. (17), $\rho^{(0)} \sim \epsilon^{1/3}$ implies $(\partial/\partial r) \sim \epsilon^{-2/3}$ which implies that the boundary layer is located radially at $r = a(1 - \epsilon^{2/3})$. Table 1 gives an accounting of the size and dependences of all quantities in the bulk plasma region and in the boundary layer.

To find the equations governing this boundary layer we will appeal to the orderings given in Table 1. The radial and perpendicular components

of Ohm's law serve to determine v_s and v_b, while the force law gives j_s and j_r. The parallel Ohm's law yields j_b, while the parallel force law links ρ, v_b, and ϕ, as do the mass and charge conservation laws.

We begin with the charge conservation, Eq. (4),

$$\frac{\partial}{\partial r}\,(r N j_r) + \frac{\partial}{\partial \theta}\,(N j_\theta) = 0 \ . \tag{19}$$

The significant order that needs to be calculated is $\epsilon^{2/3}$. Therefore we need $j_r^{(4/3)}$, $j_s^{(2/3)}$, and $j_b^{(-1/3)}$. These are, from Eq. (1),

$$j_r^{(4/3)} = -\frac{cs^2}{Br}\,\frac{\partial \rho^{(4/3)}}{\partial \theta} + \frac{cs^2}{BR}\cos\theta\,\frac{\partial \rho^{(1/3)}}{\partial \theta} + \frac{c\rho^{(1/3)}}{BR}\,v_b^{(0)^2}\sin\theta\,, \tag{20}$$

$$j_s^{(2/3)} = \frac{c}{B}\,s^2\,\frac{\partial \rho^{(4/3)}}{\partial r}\ , \tag{21}$$

and from Eq. (2),

$$j_b^{(-1/3)} = -\frac{f}{\eta r}\,\frac{\partial \phi^{(5/3)}}{\partial \theta}\ . \tag{22}$$

Combining these last three equations with Eqs. (6), (7), and (19), yields

$$\frac{\partial^2 \phi^{(5/3)}}{\partial \theta^2} = \frac{\eta c}{Bf^2}\,\frac{r^2}{R}\sin\theta\left[\frac{\partial}{\partial r}\left(\rho^{(1/3)}\,v_b^{(0)^2} + 2s^2\rho^{(1/3)}\right)\right] \ . \tag{23}$$

The leading terms from Ohm's law, Eq. (2), are

$$v_r^{(5/3)} = -\frac{c}{B_o r}\,\frac{\partial \phi^{(5/3)}}{\partial \theta}\ , \tag{24}$$

$$v_s^{(3/3)} = \frac{c}{B_o} \frac{\partial \phi^{(5/3)}}{\partial r} \quad . \tag{25}$$

The leading order parallel force law then becomes

$$-\frac{c}{B_o}\left(\frac{\partial v_b^{(0)}}{\partial r}\frac{\partial \phi^{(5/3)}}{\partial \theta} - \frac{\partial v_b^{(0)}}{\partial \theta}\frac{\partial \phi^{(5/3)}}{\partial r}\right) + \frac{f}{2}\frac{\partial [v_b^{(0)}]^2}{\partial \theta} + s^2 f \frac{\partial}{\partial \theta}(\ln \rho^{(1/3)}) = 0 \tag{26}$$

and the leading order mass continuity becomes

$$-\frac{c}{B_o}\left(\frac{\partial \rho^{(1/3)}}{\partial r}\frac{\partial \phi^{(5/3)}}{\partial \theta} - \frac{\partial \rho^{(1/3)}}{\partial \theta}\frac{\partial \phi^{(5/3)}}{\partial r}\right) + f \frac{\partial}{\partial \theta}(\rho^{(1/3)} v_b^{(0)}) = 0 \, . \tag{27}$$

Equations (23), (26), and (27) are the set of equations governing the structure of the boundary layer. They nonlinearly couple ρ, v_b, and ϕ through three partial differential equations in two variables, r and θ. Before solving this set let us verify that in the limit of returning from the boundary layer to the bulk plasma, our set reduces to one whose solutions are the bulk-plasma ρ, ϕ, and v_b. This will ensure the matching of whatever boundary layer solutions we find to the bulk-plasma solutions.

To approach the limit of bulk plasma parameters, we refer back to Table 1, along with the setting of $v_b^{(0)}(r)$ and $\phi^{(1)}(r)$ to zero to exclude unidirectional poloidal flows, which are clearly absent from Fig. 1. In this limit Eq. (23) becomes

$$\frac{\partial^2 \phi^{(2)}}{\partial \theta^2} = \frac{2\eta c}{Bf^2}\frac{r^2 s^2}{R}\sin\theta \frac{d\rho^{(0)}}{dr} \, , \tag{23'}$$

which can be integrated immediately since $\sin\theta$ is the sole θ dependence. Then Eqs. (24) and (25) yield

$$v_r^{(2)} = \frac{\eta c^2}{B^2} \frac{2s^2 r}{f^2 R} \cos\theta \left(\frac{d\rho^{(0)}}{dr} \right) \tag{24'}$$

$$v_s^{(2)} = - \frac{2\eta c^2 s^2}{B^2 R} \sin\theta \frac{d}{dr} \left(\frac{r^2}{f^2} \frac{d}{dr} \rho^{(0)} \right) . \tag{25'}$$

These are in complete agreement with the bulk plasma solutions for v_r and v_s given in Ref. 2, [Eqs. (21) and (22)]. A further consequence of taking the bulk plasma limit is that Eq. (27) becomes

$$- \frac{c}{B_o} \frac{\partial \phi^{(2)}}{\partial \theta} \frac{d\rho^{(0)}}{dr} = - f\rho^{(0)} \frac{\partial v_b^{(1)}}{\partial \theta} . \tag{27'}$$

Since $\phi^{(2)}$ is now known from Eq. (23'), Eq. (27') yields for $v_b^{(1)}$,

$$v_b^{(1)} = - \frac{2\eta c^2 s^2 r^2}{B^2 f^3 R} \left(\frac{1}{\rho^{(0)}(r)} \right) \left(\frac{d\rho^{(0)}(r)}{dr} \right) \sin\theta , \tag{27''}$$

which agrees with Ref. 2, Eq. (26). Since $v^{(2)}_{\text{poloidal}} = v_s^{(2)} + f v_b^{(1)}$, Eqs. (25') and (27'') can be combined, and yield the behavior shown in Fig. 1a. Similarly, $v^{(1)}_{\text{toroidal}} = v_b^{(1)}$ yields, via Eq. (27''), the flow behavior of Fig. 1c. Thus, our boundary layer set of equations indeed yields bulk-plasma solutions when we go to the proper bulk-plasma limit.

A very useful solution of the set of boundary layer equations (23), (26), and (27) is separable in the form

$$\rho^{(1/3)}(r,\theta) = [(a-r)/a]^2 \tilde{\rho}^{-(3/3)}(\theta) \ ,$$

$$\phi^{(5/3)}(r,\theta) = [(a-r)/a] \tilde{\phi}^{(3/3)}(\theta) \ , \qquad (28)$$

$$v_b^{(0)}(r,\theta) = \tilde{v}_b^{(0)}(\theta) \ .$$

These choices are useful, not only in that they reduce the complicated set of equations to a set of <u>ordinary</u> differential equations in θ, but also in that they satisfy the boundary conditions at $r=a$. The potential ϕ vanishes at the absorbing, conducting surface (a limiter), as does the density ρ. Note too, that the bulk-plasma density profile enters the boundary layer, dropping off quite steeply. The parabolic $\rho(r)$ in the boundary layer gently returns this steepening into a more realistic bell-shaped profile. This is shown in Fig. 4.

V. POLOIDAL STRUCTURE: SUBSONIC

Before moving on to solve for the poloidal structure of the boundary layer, it is convenient to put the set of equations for the separable solution into dimensionless form. Let

$$\eta_o \equiv \frac{\eta c^2}{B^2} \frac{s}{a} \frac{\rho(0)}{f^4} \frac{a}{R} \ , \qquad (\ )_\theta \equiv \frac{\partial (\ )}{\partial \theta} \ ,$$

and introduce for the θ dependent factors of the separated solutions,

$$v \equiv \frac{\tilde{v}_b^{(0)}}{s} , \qquad \phi \equiv \frac{c}{Ba} \frac{\tilde{\phi}^{(3/3)}}{fs} , \qquad \rho \equiv \frac{f\tilde{\rho}^{(-3/3)}}{\rho(0)} , \quad m \equiv \phi + v . \tag{29}$$

All quantities are now of order $\epsilon^0 = 1$. Using Eqs. (23), (26), (27), (28), and (29) we obtain, after some rearrangement of (26) and (27),

$$\rho_\theta = 2\rho\psi m/(m^2 - 1) \tag{30}$$

$$v_\theta = -2\psi/(m^2 - 1) \tag{31}$$

$$\phi_\theta \equiv \psi \tag{32}$$

$$\psi_\theta = 2\eta_o(2 + v^2)\rho \sin\theta \tag{33}$$

Note the denominator has a singularity at $m = \pm 1$, "mach one". In unscaled form this corresponds to $v_{poloidal}$ equalling the reduced sound speed[8] fs. This speed corresponds to the "slow hydromagnetic wave" propagating in the θ direction. Let $b^2 = B^2/4\pi\rho$ and $b_n^2 = b_\theta^2 = f^2 b^2$, then

$$C_{sl_n}^2 = \frac{1}{2}\left\{ (s^2 + b^2) - [(s^2 + b^2)^2 - 4s^2 b_n^2]^{1/2} \right\}$$
$$\approx \frac{s^2 b_n^2}{s^2 + b^2} \approx s^2 f^2 . \tag{34}$$

A perturbation will not propagate in a plasma that is flowing at this speed and thus a standing shock can be formed. This, then, is the significance of the singularity in the denominator.

Since Eqs. (30) - (32) are autonomous we can actually solve for ρ and ϕ in terms of v. Adding Eqs. (31) and (32), we obtain

$$m_\theta = \frac{(m^2 - 3)}{(m^2 - 1)} \phi_\theta \ .$$

The integration can be performed straightforwardly, yielding

$$\phi = m - \frac{1}{\sqrt{3}} \ln \frac{\sqrt{3} + m}{\sqrt{3} - m} \ , \tag{35}$$

and thus

$$m = \phi + v = \sqrt{3} \tanh \left(\frac{\sqrt{3}}{2} v \right) \ . \tag{36}$$

In determining constants of integration we have assumed that $m = v = \phi = 0$ at $\theta = 0$, and π. This choice is motivated by the physics of the bulk plasma Pfirsch-Schlüter convective flows as shown in Fig. 1 (a and c), ($m = v = 0 \Rightarrow \phi = 0$).

Next we divide Eq. (30) by Eq. (31), and obtain

$$\frac{d(\log \rho)}{dv} = -m = -\sqrt{3} \tanh \left(\frac{\sqrt{3}}{2} v \right) \ ,$$

which can also be solved explicitly, yielding

$$\rho = \rho(v=0) \operatorname{sech}^2 \left(\frac{\sqrt{3}}{2} v \right) \tag{37}$$

at $v_{crit} = \pm 0.76034 \ldots$, $m = \pm 1$, and $\rho = (2/3)\rho(0)$. Thus, we need only solve a final reduced set

$$\begin{aligned} v_\theta &= -2\psi / \left(3 \tanh^2 \left(\frac{\sqrt{3}}{2} v - 1 \right) \right. \\ \psi_\theta &= 2\eta_o \rho(0)(2 + v^2) \operatorname{sech}^2 \left(\frac{\sqrt{3}}{2} v \right) \sin\theta \ . \end{aligned} \tag{38}$$

In general, this nonlinear set must be integrated numerically. We can find an analytic solution in the limit of small $\rho(0)$.

We call this the subsonic solution in which $m_{max} \ll 1$ ($v_{max} \ll v_{crit}$). Since v will be small, we take $(2+v^2)\,\mathrm{sech}^2\,[(\sqrt{3}/2)v] = 2$, let $4\eta_o\rho(0) \equiv \delta \ll 1$ and obtain

$$\begin{aligned} \psi &\approx -\delta\cos\theta\,, \\ v &\approx -2\delta\sin\theta\,, \\ \phi &\approx -\delta\sin\theta\,, \\ m &\approx -3\delta\sin\theta\,, \\ \rho &\approx \rho(0)\,. \end{aligned} \tag{39}$$

These are pictured in Fig. 5. Note that these solutions obey the boundary conditions $m = v = \phi = 0$ at $\theta = 0, \pi$ as well as periodicity constraints. Note also the natural way in which this poloidal behavior matches qualitatively back into the bulk plasma flow pattern. This is shown in Fig. 7. Quantitatively, Eq. (39) does not agree with Eqs. (23') - (27') because of the additional assumptions introduced in forming the separated solution. The relations between these various solutions will be discussed in Sec. VIII.

VI. POLOIDAL STRUCTURE - TRANSONIC

Our subsonic results are not the only type of solutions of the non-linear set Eq. (38). We now explore solutions with transonic behavior. Figure 7 deals with the four possible varieties of solutions when the Mach number m is close to unity. Case (a) is a subsonic solution with maximum velocity slightly less than the reduced sound speed. This type is characterized by $|v(\theta_{crit})| < v_{crit}$ where v_{crit} is defined below Eq. (37) and $\theta = \theta_{crit}$ is the point at which $\psi(\theta_{crit}) = 0$. The $(b)_+$ solution is the limit as $v(\theta_{crit}) \rightarrow v_{crit}$. The $(b)_-$ solution is transonic. Analysis of the set Eq. (38) shows that if $v(\theta_{crit}) = v_{crit}$ we obtain $v_\theta = \pm[\psi_o(\theta_{crit})]^{1/2}$, with the $\pm$ signs corresponding to the $(b)_\pm$ curves. Either solution is possible, depending on global conditions. Finally, the curve (c) has $|v_\theta| = \infty$ at $v = v_{crit}$, and implies the possibility of shock solutions. The need for shock solutions comes from the fact that any solution following a $(b)_-$ path goes right through v_{crit} and continues supersonically, never to return the velocity back to zero. But $v = 0$ at $\theta = 0$ and π. Therefore, there must be a sudden jump back to a different type of solution, for which case (c) is a perfect candidate, that will return v to zero. This is shown in Fig. 10 b.

The borderline between shock and subsonic solutions is the aforementioned $(b)_+$ or zero shock solution. It can be described quite accurately as

$$v = \frac{2 v_{crit}}{\pi} \theta$$

$$\psi = \frac{v_{crit}}{\pi} \left[1 - 3 \tanh^2 \left(\sqrt{3} \frac{v_{crit}}{\pi} \theta\right)\right] , \qquad (40)$$

in the region $0 \leq \theta \leq \pi/2$. Then reflecting symmetrically around $\pi/2$, and then antisymmetrically around π reveals the full zero shock solution as shown in Fig. 8. It is noteworthy that the three possible solutions mentioned, subsonic, zero shock, and shock bear a striking resemblance to classical one-dimensional compressivle fluid in a converging-diverging nozzle.[9]

Returning now to the shock solutions, we must find a recipe that dictates where and how to jump from the supersonic to subsonic branch. The obvious physical constraints are mass- and momentum-flux conservation across the poloidal shock. In deriving these conditions, the $\partial/\partial\theta$ terms will predominate, yielding from Eq. (3)

$$\frac{\partial}{\partial\theta} (\rho v_{\text{poloidal}}) = 0 ,$$

or in our scaled units

$$[\![\rho m = 0]\!], \tag{41}$$

where the brackets denote a jump across the shock. The momentum flux conservation, Eq. (26) yields

$$\frac{m \partial v}{\partial \theta} + \frac{1}{\rho} \frac{\partial \rho}{\partial \theta} = 0 ,$$

which, with Eq. (41) reduces to

$$[\![\frac{1}{m} + v]\!] = 0 . \tag{42}$$

It is helpful to plot ρm and $(1/m) + v$ as functions of v in Fig. 9a, and then as a function one of the other in Fig. 9b.

It would seem, at first glance, that the subsonic and supersonic branches intersect at only one point; $|m| = 1$, thus allowing only a zero shock solution. However, the $\rho(v=0)$ factor in ρ, Eq. (37), allows <u>two</u> values, $\rho(\theta = 0)$ and $\rho(\theta = \pi)$. With $\rho_\pi > \rho_o$ we have Fig. 10a. We begin at $\theta = \pi$ along the $\rho_\pi m$ curve, (1), pass transonically through mach one,(2) and finally jump back to the subsonic solution (3), that returns us, along $\rho_o m$ to $\theta = 0$. In real space this is shown in Fig. 10b. Thus, we have ensured that the periodicity and boundary conditions on v (and ϕ and m) be fulfilled.

Thus, the scenario for shock fitting is as follows. We first choose $\rho_o(\theta = 0)$(subscript o denotes the downstream solution that includes $\theta = 0$, and subscript π denotes the upstream solution). This generates a single curve in the $[\rho m, (1/m) + v]$ plane, independent of $\psi(\theta \equiv 0)$, such as Fig. 10a. Next choose any $\rho_\pi(\theta = \pi) \geqq \rho_o(\theta = 0)$. This will generate another curve that intersects the first, as in Fig. 10a. The intersection point defines a unique pair (v_{sup}, v_{sub}), across which the shock will stretch, and, by construction, preserve the mass and momentum fluxes.

Once $\rho_\pi(\theta = \pi)$ is chosen, $\psi_\pi(\theta = \pi)$ will then determine $v_\pi(\theta)$ and $\psi_\pi(\theta)$ for all θ. However, there is only one $\psi_\pi(\theta = \pi)$ that determines a $\psi_\pi(\theta)$ satisfying $\psi_\pi = 0$ when $v_\pi = v_{crit}$, the transonic flow condition. With $\rho_\pi(\theta = \pi)$ given, and $\psi_\pi(\theta = \pi)$ now determined, so is $v_\pi(\theta)$.

Where $v_\pi(\theta) = v_{sup}$, that is the shock position θ_s (as in Fig. 10b). Once θ_s is determined, we know exactly where v_{sub} must be. Our $v_o(\theta)$ solution must therefore satisfy $v_o(\theta_s) = v_{sub}$. There is only one $\psi_o(\theta=0)$ that can generate such a solution. There are now two free parameters, $\rho_o(0)$ and $\rho_\pi(\pi)$. In general, one would expect to have two more jump conditions across the shock so that there is one corresponding to each derivative in the set, Eqs. (30) - (33). However, these conditions are not consistent. The reason is that the quantity $\int \eta j^2 d\tau$ represents energy lost from the system of Eqs. (1) - (4). Thus, strong shocks must be associated with an energy loss that is not consistent with the magnitude of time derivatives that have been assumed in this paper. However, consistent small amplitude shocks can be found where the onus of matching the additional jump conditions can be placed on terms that are higher order in the shock strength.

Thus, let us investigate "small-shock" solutions in which the shock strength is of order $\delta \sim \epsilon^{1/3} \ll 1$. Then $m \approx -1 \pm \delta$, and $\rho_o(\theta = 0)$ has the value required for v to reach the $(b)_+$ solution of Fig. 7. For Eqs. (36) and (42) to be fulfilled through and including orders δ^3, we find

$$v = v_c \pm \delta - \frac{2}{3}\delta^2 ,$$

$$m = -1 \pm \delta - \frac{1}{6}\delta^2 \mp \frac{2}{3}\delta^3 , \qquad (43)$$

$$\rho_\pi(\theta = \pi) = \rho_o(\theta = 0)(1 + 2\delta^3) .$$

Thus when we eventually determine δ as a function of $(a - r)$, we will

determine $\rho_\pi (\theta = \pi)$, and then the shock will be fully determined. Another ramification of these solutions is that ϕ is really conserved as seen below, but using Eq. (36), $[\![\phi]\!] = |m - v| = 4/3\, \delta^3$. Thus, there must be corrections to Eq. (36) via higher order equations. This brings us to the next task, which is solving for the actual shock structure.

Since $j_r \sim \partial \rho / \partial \theta$ (force law), we expect it to grow large within the poloidal shock. For maximal ordering, since $v_s^{(1)} = (c/B)(\partial \phi^{(5/3)}/\partial r) + (\eta c/B_o)\, j_r$ (Ohm's law), and $\eta \sim \epsilon^3$, we demand that j_r grow to be ϵ^{-2} within the shock. Thus, the mass continuity equation, Eq. (41), now becomes, in dimensionless form

$$\rho \left(\phi + v - x^2 \eta_o \epsilon^{7/3} \rho_\theta \right) = K_1 \tag{44}$$

where K_1 is a constant of integration and $x \equiv (r - a)\, \epsilon^{-2/3}$. While the parallel momentum law, Eq. (42), remains

$$\rho + K_1 v = K_2 \quad , \tag{45}$$

with K_2 another constant of integration. We solve these last two equations for the small shock solutions, Eq. (32), in which ϕ and ψ are both constant across the shock. In this limit the leading order of Eq. (44) is a constant, so the calculation is carried to order δ^2. These yield

$$\rho_o = \frac{2}{3} \rho_o \ (\theta = 0) \qquad K_1 = \rho_o \left(-1 + \frac{3}{2} \delta^2\right), \qquad K_2 = \rho_o \left(1 - v_c + \frac{3}{2} v_c \delta^2\right).$$

Upon manipulation, Eqs. (44) and (45) reduce to

$$\int \frac{\rho_o \, d\rho}{\left[\rho - (1 - \delta^2)\rho_o\right]^2 - \rho_o^2 \delta^2} = \frac{(\theta - \theta_o)\epsilon^{-7/3}}{\eta \rho_o x^2} \quad .$$

This is a standard integral whose solution yields

$$\rho = \rho_o \left[1 - \delta \tanh\left(\frac{(\theta - \theta_o)\delta\epsilon^{-7/3}}{\eta_o \rho_o x^2}\right)\right] . \tag{46}$$

We find a shock thickness "$\delta\theta$" $\sim \epsilon^{7/3}/\delta \sim \epsilon^{6/3}$. Note that $j_r \sim \rho_\theta^{(1/3)} \sim (\delta\epsilon^{-7/3})\,\delta\epsilon^{1/3} \sim \delta^2\epsilon^{-2}$.

We have also solved for the shock structure by including viscosity in Ref. 7 . Because this result is not very different, we have left out the analysis here.

The physical significance of the shock solutions have been described earlier in this section when we showed why mach one was a critical velocity. The poloidal structure shown in Fig. 11 matches onto the bulk plasma behavior quite naturally, as it did for the subsonic case, if the shock begins at zero strength as we first enter the boundary layer. In the next section, we will prove that it so, by investigating the radial behavior of δ , the shock strength.

VII. DIFFUSION

Since our goal is that of finding the radial behavior of the shock strength $\delta \sim \epsilon^{1/3}$, it is clear that we must look at the next order boundary layer equations (smaller than the leading order ones by $\epsilon^{1/3}$). With the notation

$$\rho^{(1/3)} \equiv (r-a)^2 \rho, \qquad v_b^{(0)} \equiv v, \qquad \phi^{(5/3)} \equiv (r-a)\phi, \qquad \frac{\partial(\,)}{\partial r} \equiv (\,)_r,$$

$$\rho^{(2/3)} \equiv \hat{\rho} \qquad v_b^{(1/3)} \equiv \hat{v}, \qquad \phi^{6/3} \equiv \hat{\phi}, \qquad \frac{\partial(\,)}{\partial \theta} \equiv (\,)_\theta,$$

we obtain the equivalents of Eqs. (23), (26), and (27):

$$\hat{\phi}_{\theta\theta} = \frac{\eta a^2}{f(a)^2} \frac{c}{BR} \sin\theta \left[(2s^2 + v^2)\hat{\rho}_r + 4(r-a)\rho v\hat{v} + 2(r-a)^2 \rho v \hat{v}_r \right], \tag{47}$$

$$\frac{c}{B}\rho\left[-\hat{\phi}_r v_\theta + (r-a)\phi\hat{v}_r - \phi\hat{v}_\theta\right] - s^2 f(a)\hat{\rho}_\theta + \frac{5}{3}\hat{\rho}(\phi v_\theta) - f(a)\left[\hat{\rho} v v_\theta + (r-a)^2 (v_\theta \hat{v} + v\hat{v}_\theta)\right] = 0, \tag{48}$$

$$-\frac{c}{B}\left[2(r-a)\rho\hat{\phi}_\theta - (r-a)^2 \rho_\theta \hat{\phi}_r\right] + -\frac{c}{B}\left[\hat{\rho}_r (r-a)\phi_\theta - \hat{\rho}_o \phi\right] + f(a)(r-a)^2 (\rho\hat{v})_\theta + f(a)(\hat{\rho} v)_\theta = 0. \tag{49}$$

If we attempt a separable solution of the form $\hat{\rho} = (r-a)^{n_\rho} \tilde{\rho}(\theta)$, etc., we find that $n_\rho = n_\phi + 1 = n_v + 2$. Though this is the same relationship

that held for the leading order solution, there n_v was determined to be zero. Here it is undetermined, and thus we have a "floating" behavior in (r-a) for all three functions. This fact will play a crucial role in what is to soon folow.

We now turn to finding the diffusion for our weak shock solutions. The diffusion equation is merely Eq. (3) averaged over θ:

$$\frac{\partial \bar{\rho}}{\partial t} = -\frac{1}{r}\frac{\partial}{\partial r}\, r \oint (\rho N v_{rad})\, d\theta \tag{50}$$

where a bar denotes a θ average. It is straightforward to show that for a zero shock solution, the right-hand side yields the Pfirsch-Schlüter result

$$r\,(r-a)^2 \frac{\partial}{\partial t}\, \overline{\tilde{\rho}^{-(3/3)}}(\theta) = -\frac{\partial}{\partial r}\left[\, r(r-a)^3 \;\; K_2 \,\right] \tag{51}$$

where

$$K_2 = -\frac{2\eta c^2 s^2}{B^2}\left(\overline{\tilde{\rho}^{-(3/3)}(\theta)}\right)^2 \;\; (1+2q^2) = \theta(\epsilon)\ .$$

Our task is to calculate additional terms due to the shock. In our dimensionless notation we are considering $\oint \rho\,\psi\, d\theta$. Normally this would vanish, as $\rho \sim 1+\cos 2\theta$ and $\psi \sim \cos\theta$. However, due to the shock, the symmetry is broken in the small regions (of width $\sim \delta$) around $\theta = \pi/2$, $3\pi/2$. A close-up of those regions is shown in Fig. 12. Calling $(\partial\psi/\partial\theta)(\theta - \pi/2) \equiv \Delta^2$, $y = \theta - \pi/2$, we obtain

$$\rho\,(y) = (2/3)\rho_o(\theta = 0)[1 + (\delta/\epsilon)\,y]\ ,$$
$$\psi = \Delta^2 y\ . \tag{52}$$

But we know that $v_{sub,\,sup} = v_{crit} \pm \Delta y$, implying that $\delta = \epsilon\Delta$. Then

$$\oint \rho\psi d\theta = \int_{-c}^{\epsilon} \rho_o\,[2/3\,(1 + \Delta y)]\,(\Delta^2 y)\,dy \sim \delta^3\rho_o\ . \tag{53}$$

There is another term due to the shocks. From Eqs. (43) and (46) we can write ϕ as

$$\phi = \phi_c + 2/3\,\delta^3 \tanh \frac{(\theta - \theta_o)\,\delta\epsilon^{7/3}}{x^2\eta_o\rho_o}$$

since $1/3\,\delta^3$ is the jump in ϕ across the shock. Then

$$\psi = \phi_o = \frac{2}{3}\,\frac{\delta^4\epsilon^{-7/3}}{x^2\eta_o\rho_o}\ \operatorname{sech}^2\left(\frac{(\theta - \theta_o)\delta\epsilon^{-7/3}}{x^2\eta_o\rho_o}\right)\ . \tag{54}$$

Using $\rho = \rho_o(\theta = 0)(2/3)$, we obtain

$$\oint \rho\psi d\theta = \frac{2}{3}\rho_o(\theta = 0)\int_{-\infty}^{\infty} \frac{2}{3}\,\frac{\delta^4\epsilon^{-7/3}}{\eta_o\rho_o x^2}\ \operatorname{sech}^2(y)\ \frac{x^2\eta_o\rho_o}{\epsilon^{-7/3}\delta}\ dy \sim \rho_o\delta^3\ . \tag{55}$$

Putting Eqs. (50), (51), (53), and (55) together, we obtain

$$r\,(r-a)^2\,\frac{\partial\overline{\tilde{\rho}^{(-3/3)}(\theta)}}{\partial t} = -\frac{\partial}{\partial r}\,[(r-a)^3\,(K_1\delta^3 + K_2)]\ . \tag{56}$$

All three terms on the right-hand side are $O(\epsilon)$ since $\delta \sim \epsilon^{1/3}$. It is clear from Eq. (56) that

$$\frac{\partial \epsilon^{-1}}{\partial t} \sim \epsilon \qquad \text{or} \qquad \frac{\partial}{\partial t} \sim \epsilon^{2} \quad . \tag{57}$$

This contradicts our assumptions of a plasma slowly decaying by classical diffusion on a time scale $(\partial/\partial t) \sim \eta \sim \epsilon^{3}$. In other words, the boundary layer collapses much faster than the interior plasma, bringing into question the entire analysis.

However, this "catastrophe" can be prevented by making what is inside the bracket on the right-hand side of Eq. (56) – a constant. This is the toroidal analogy of what was done in the cylindrical case when the diffusion near the edge was calculated. Recall Eqs. (13) - (17) in which we set $(d/dr)[\rho(d\rho/dr)]$ to zero, or $\rho(d\rho/dr) =$ constant.

The freedom in the radial variation of the shock strength $\delta (= v^{(1/3)})$, as discussed at the beginning of this section, now enters to play a crucial role. It allows us, here, to use the technique of "setting the bracket equal to a constant", and obtaining

$$\delta^{(1/3)} = (\text{constant}) \left(\frac{a^{3} \epsilon^{2}}{(a-r)^{3}} - 1 \right)^{1/3} \epsilon^{1/3} \quad . \tag{58}$$

At the onset of the boundary layer $[r = a(1 - \epsilon^{2/3})]$ we have $\delta = 0$, as required to match onto the shockless bulk plasma interior. Throughout the boundary layer δ grows, until at $r = a(1 - \epsilon)$ δ becomes finite and the analysis breaks

down. This is consistent with the "floating" radial behavior of the higher order quantities, since if $v^{(1/3)} \sim \epsilon/(r-a)$, then at $r = a(1-\epsilon)$, $v^{(1/3)} \sim \epsilon^0 \sim v^{(0)}$ and the analysis breaks down. Similar arguments for ρ and ϕ show a similar breakdown at $r = a(1-\epsilon)$. It should be noted that by then ρ becomes small, of order ϵ.

VIII. CONCLUSIONS

Conditions near the boundary of a diffusing, large aspect ratio, toroidal plasma have been considered. Near the plasma edge, density gradients increase, as was shown in Sec. III. Further, secondary flow along the field lines also increases. Throughout most of the plasma these effects remain small enough that they can be treated as perturbations. This was calculated in Ref. 2. These perturbation results, when combined with the calculation of Sec. III, lead to the estimate that when $a - r \sim \epsilon^{2/3}$, where ϵ is the inverse toroidal aspect ratio, density variations, and secondary flows become finite and perturbation theory is no longer valid. A set of nonlinear equations governing this nonlinear behavior was derived in Sec. IV.

The most significant solution of these equations is that containing a weak shock, discussed in Sec. VI. Here, there is a layer where the maximum flow velocity is very close to the sonic speed, and the density profile is self similar and falls off as $(a-r)^2$. The amplitude of the weak shock increases toward the plasma boundary, but it is too weak to have a direct effect on the density and velocity profiles.

Between the bulk plasma, where perturbation theory is valid, and the weak shock layer, there is a region that bridges between these two. Exact solutions of the coupled nonlinear set, Eqs. (23), (26), and (27), have not been found that cover this, but from approximate solutions[7] it is clear that there is no new interesting physics going on. The subsonic solutions of Sec. V provide a model for this region. While the amplitude of the subsonic solution will increase as the wall is approached, contrary to the separable assumptions of Sec. V, this will not have a strong effect on the profiles of Fig. 5. From Eqs. (23') - (27') it is clear that these solutions merge smoothly into the bulk plasma region.

Similarly, outside the weakshock layer, there appears to be another region of rapid variation. By continuity with the weakshock region, shocks will be of finite strength here, and perhaps particular details of the plasma-wall interaction will be important.

A broader view of the diffusion can be obtained by examining the energy relation. A direct consequence of Eqs. (1) - (4) is

$$\frac{\partial}{\partial t}\left[\frac{1}{2}\rho v^2 + s^2\rho \ln \rho/\rho_o\right] + \nabla\cdot\left[\rho v\left(\frac{1}{2}v^2 + s^2 \ln \rho/\rho_o + s^2\right) + j\phi\right] + \eta j^2 = 0 \tag{59}$$

where ρ_o is an arbitrary constant.

Thus, in this model, Ohmic dissipation represents an energy loss from the system. There is a close relation between this loss of energy and

the energy change associated with the decrease in plasma density. In particular, consider a region near the plasma boundary. Mass and energy, evicted from the central regions by diffusion, stream through this layer with magnitudes that are large compared to the resident population. Thus, we have found throughout this paper the condition that the mass flux be constant, independent of radius,

$$\frac{\partial}{\partial r} \oint \rho v_r \, d\theta = 0 ,$$

so that the boundary layer is not violently disrupted by local variations in the flux.

A similar relation for the energy flux can be found by integrating Eq. (59) over a surface of constant r. We find approximately,

$$\frac{\partial}{\partial r} \int \rho v_r \ln (\rho/\rho_o) \, d\theta + \oint \eta j^2 \, d\theta = 0 .$$

Clearly, comparing these last two results, Ohmic dissipation must increase near the plasma boundary where the density decreases and the slope of $\ln \rho$ increases. When conditions allow the formation of a weak shock, there is a new, and very efficient, source of energy dissipation. Density gradients are smaller here, because they are not needed to produce the required dissipation. Thus, the plasma profile becomes bell shaped, as in Fig. 4.

The effect of this bell shaped profile is to decrease the volume available for the confinement of the high density plasma. Thus dissipation associated with plasma flow can be important for confinement. Further, it

can have a strong influence on the poloidal variation of plasma parameters near the edge, and thus affect boundary conditions and plasma wall interactions.

ACKNOWLEDGMENTS

We thank E. A. Frieman and J. L. Johnson for critically reading this paper, and J. M. Finn and S. C. Jardin for helpful discussions. We are grateful to Dr. Shafranov for permission to reproduce Fig. 1.

This work was supported by U. S. Energy Research and Development Administration Contract E(11-1)-3073.

REFERENCES

*Present Address: Lawrence Livermore Laboratory, L-545, P. O. Box 808, Livermore, CA 94550.

[1] B. J. Green, Nucl. Fusion 12, 475 (1972).

[2] J. M. Greene, J. L. Johnson, K. E. Weimer, and N. K. Winsor, Phys. Fluids 14, 1258 (1971).

[3] D. Pfirsch and A. Schlüter, Max-Planck Institute Report No. MPI/PA/7/62 (1962); also, M. D. Kruskal and R. M. Kulsrud, Phys. Fluids 1, 265 (1958).

[4] G. Knorr, Phys. Fluids 8, 1334 (1965).

[5] C. L. Longmire, Elementary Plasma Physics (Wiley, New York, 1963), p. 228.

[6] N. K. Winsor, J. L. Johnson, and J. M. Dawson, J. Comp. Phys. 6, 430 (1970).

[7] M. D. Rosen, Ph. D. Thesis, Princeton University, 1976.

[8] T. Taniuti, Phys. Rev. Letters 25, 1478 (1970).

[9] R. Courant and K. D. Friedrichs, Supersonic Flow and Shock Waves (Interscience; N. Y., 1948), p. 249.

[10] R. G. Grimm and J. L. Johnson, Plasma Physics 14, 617 (1972).

TABLE 1.

Variable	Bulk Plasma	Boundary layer
r	$0 \leq r \leq a\,(1-\epsilon^{2/3})$	$a(1-\epsilon^{2/3}) \leq r \leq a$
ρ	$\epsilon^{o}(r)+\epsilon^{1}(r,\theta)$	$\epsilon^{1/3}(r,\theta)$
v_r	$\epsilon^{2}(r,\theta)$	$\epsilon^{2}(r,\theta)$
v_s	$\epsilon^{1}(r)+\epsilon^{2}(r,\theta)$	$\epsilon^{5/3}(r,\theta)$
v_b	$\epsilon^{o}(r)+\epsilon^{1}(r,\theta)$	$\epsilon^{o}(r,\theta)$
j_r	$\epsilon^{1}(r,\theta)$	$\epsilon^{1/3}(r,\theta)$
j_s	$\epsilon^{o}(r)+\epsilon^{1}(r,\theta)$	$\epsilon^{-1/3}(r,\theta)$
j_z	$\epsilon^{o}(r,\theta)$	$\epsilon^{-1/3}(r,\theta)$
ϕ	$\epsilon^{1}(r)+\epsilon^{2}(r,\theta)$	$\epsilon^{1}(r)+\epsilon^{5/3}(r,\theta)$

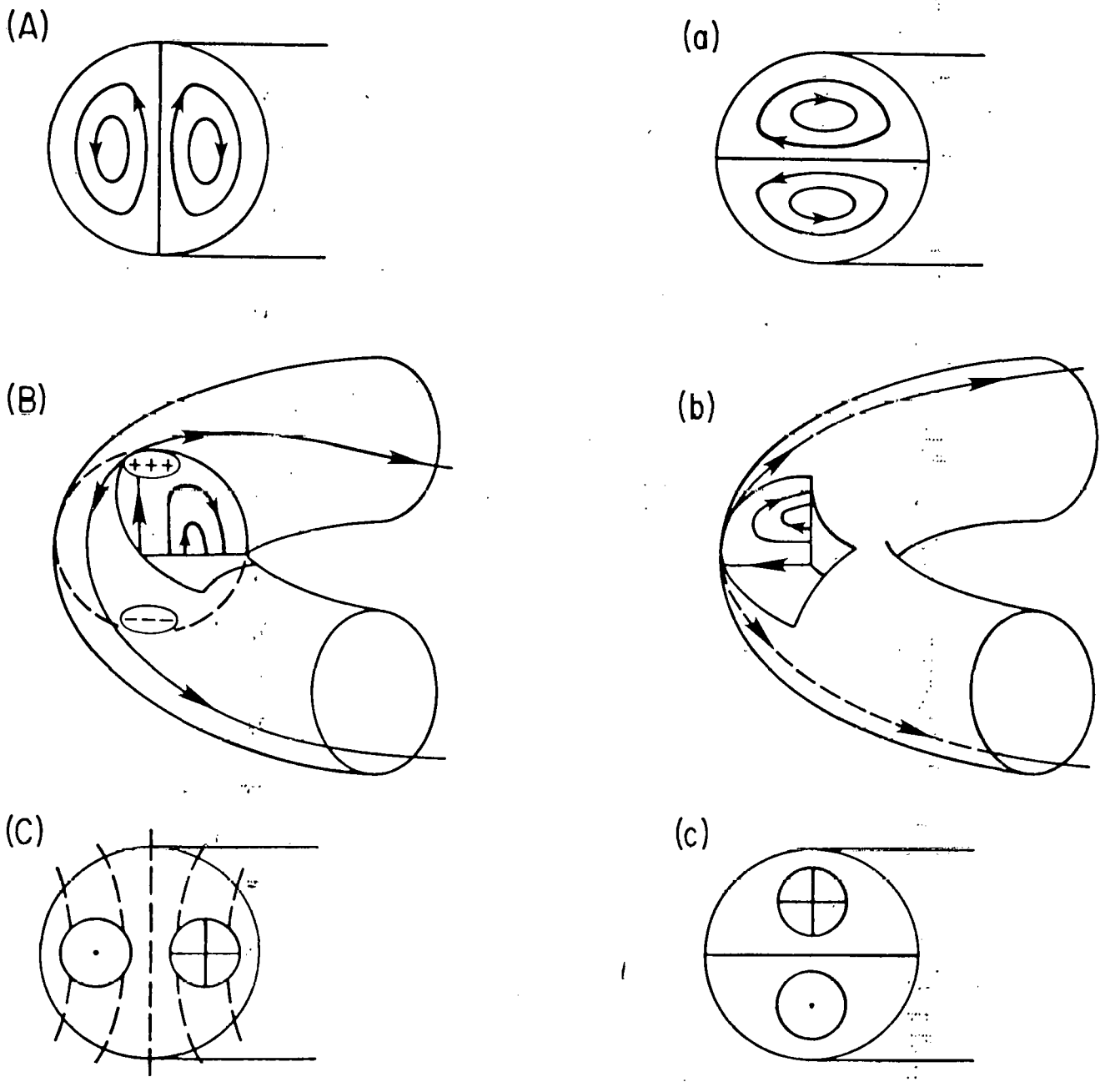

762290

Fig. 1. Pfirsch-Schlüter convection patterns. Particle drifts are sign dependent (B) causing neutralizing currents to flow (A) and (C). Resistivity prevents total neutralization, thus creating $\vec{E}\times\vec{B}$ drifts (b) shown in poloidal (a) and toroidal (c) projections.

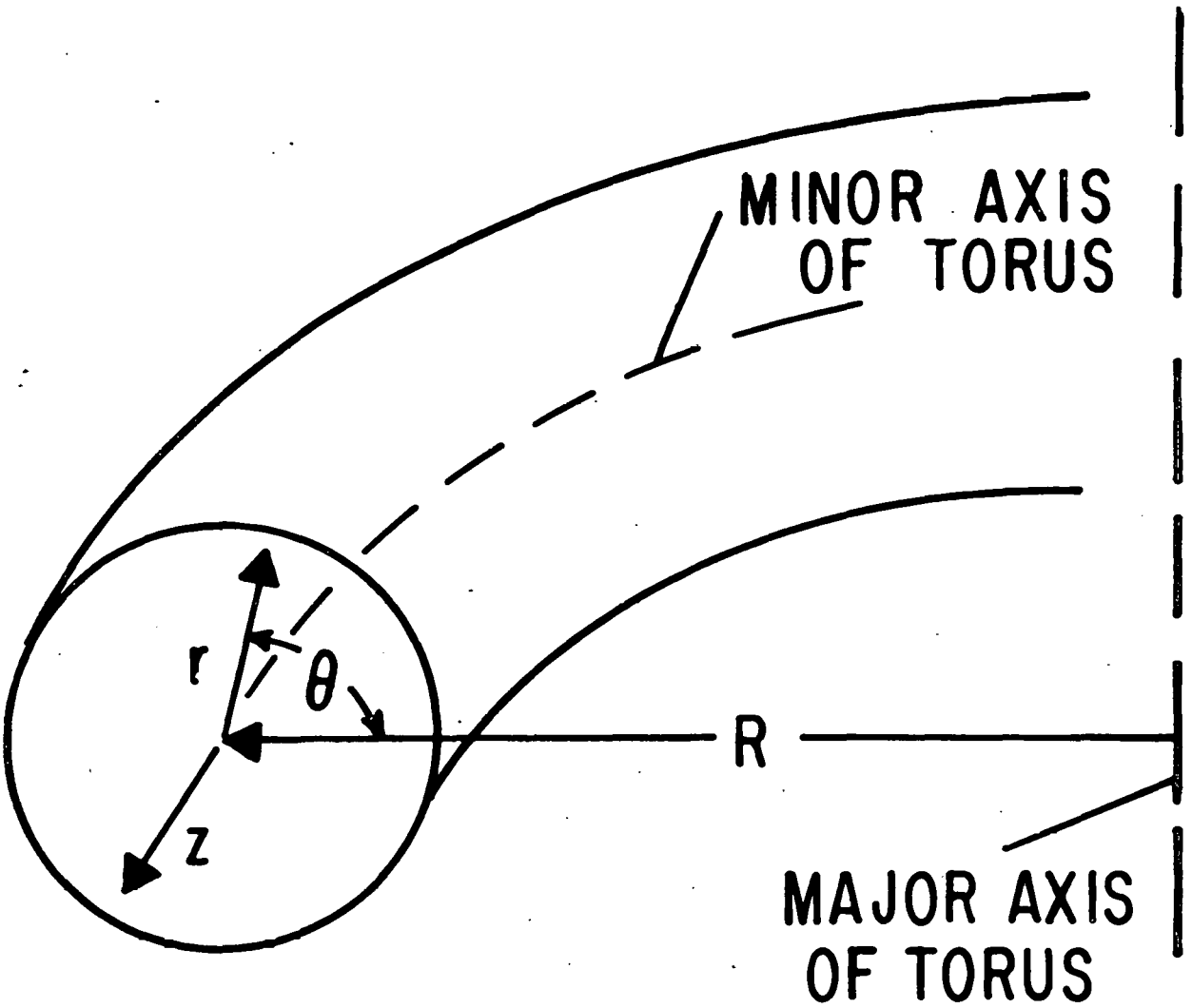

682150

Fig. 2. The (r,θ,z) toroidal coordinate system.

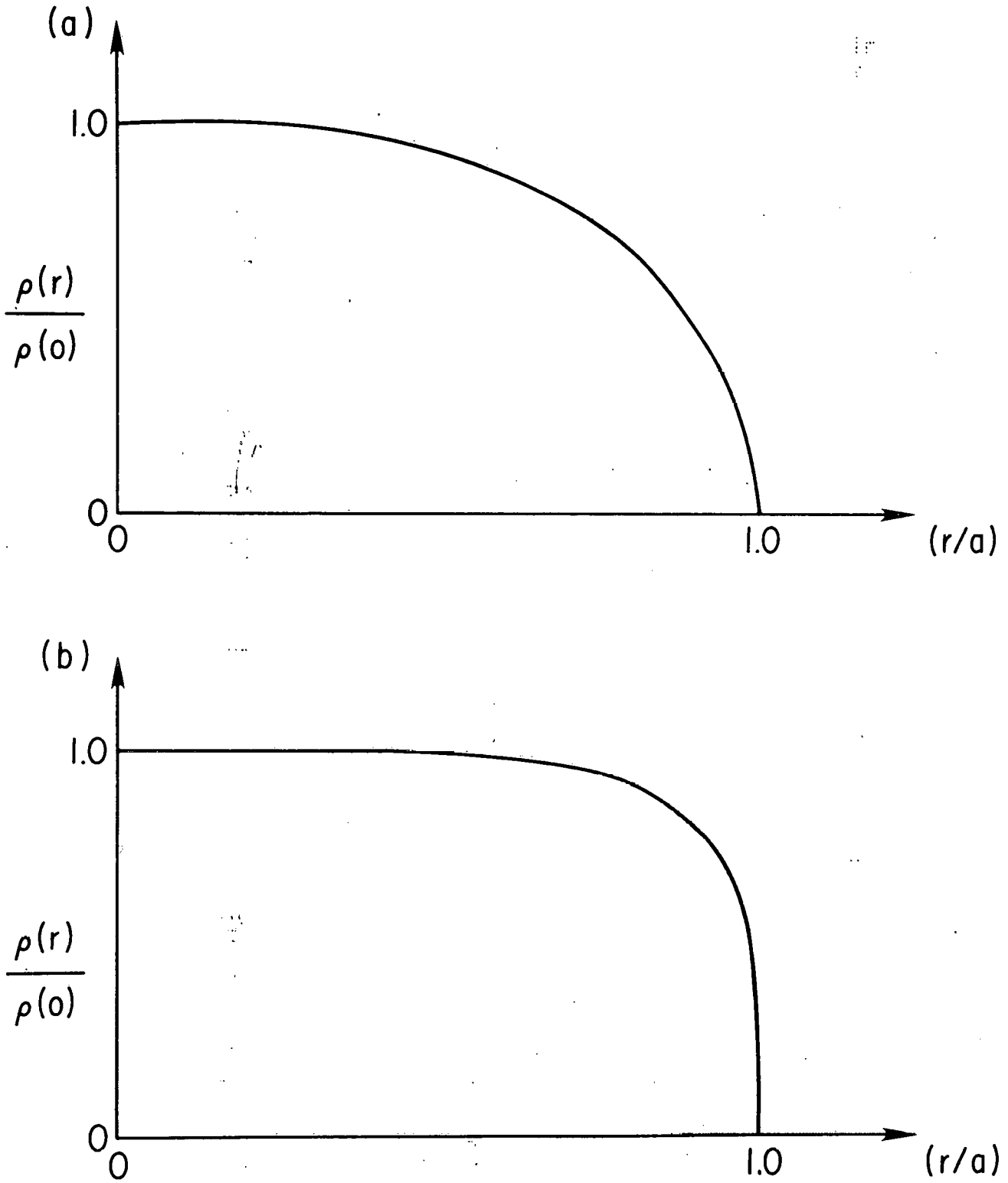

762292

Fig. 3. (a) Radial profile of density for the similarity solution of diffusion equation. (b) Radial profile of density for plasma supported by external sources.

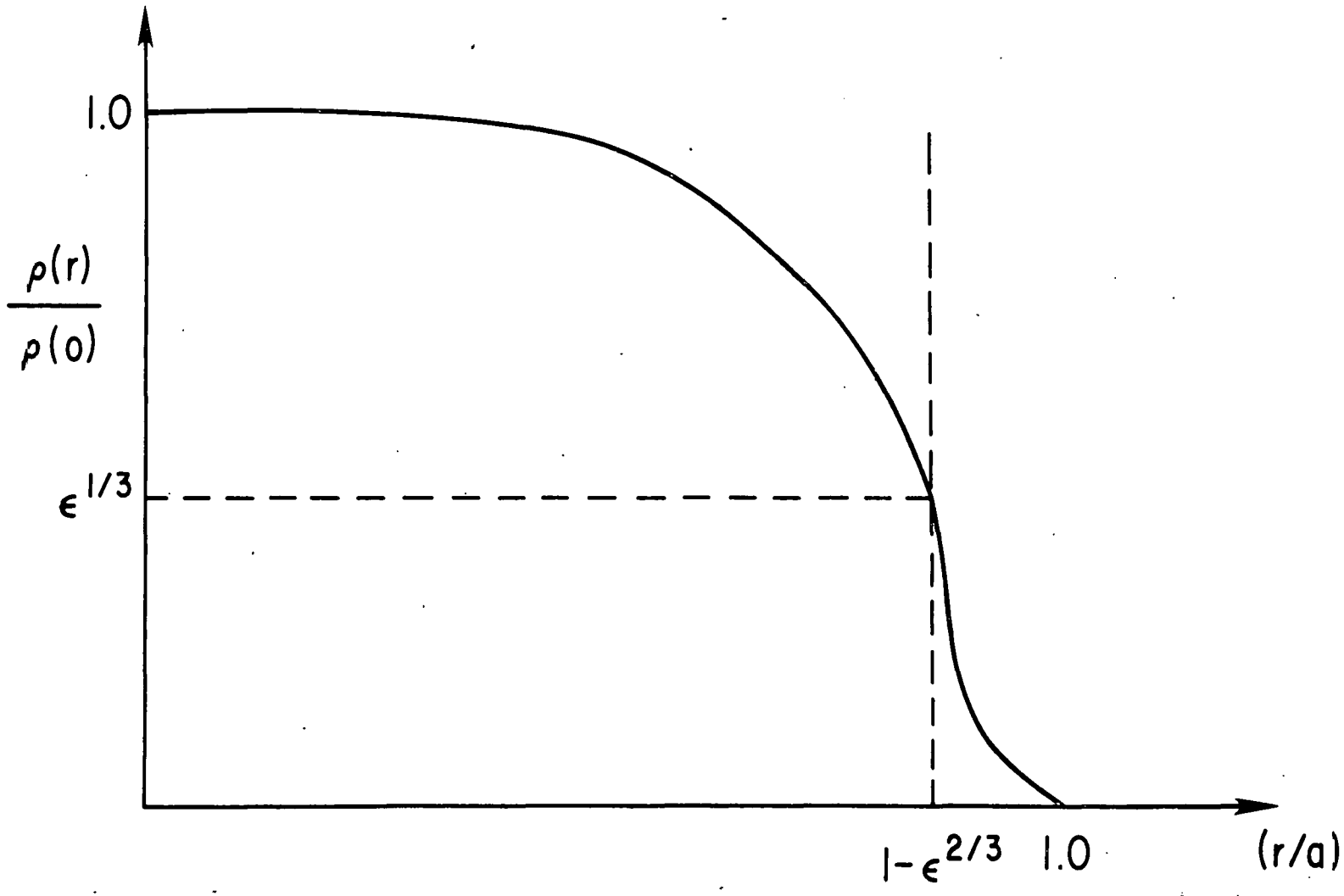

762288

Fig. 4. Modification of steep density profile in bulk plasma due to boundary layer.

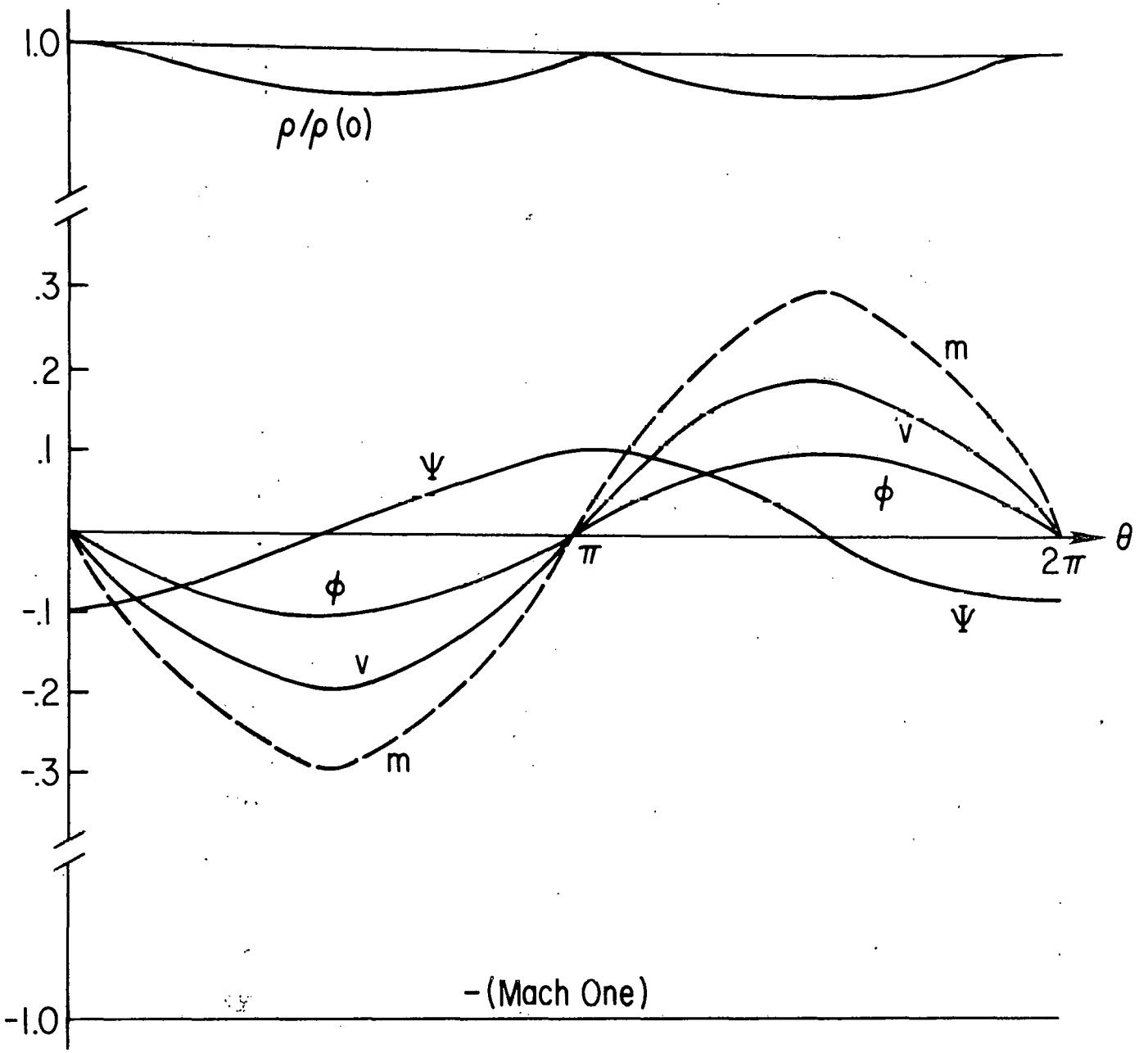

762265

Fig. 5. Subsonic solution for θ dependences of parallel flow (v), potential (ϕ), poloidal flow (m), radial flow (ψ), and density (ρ).

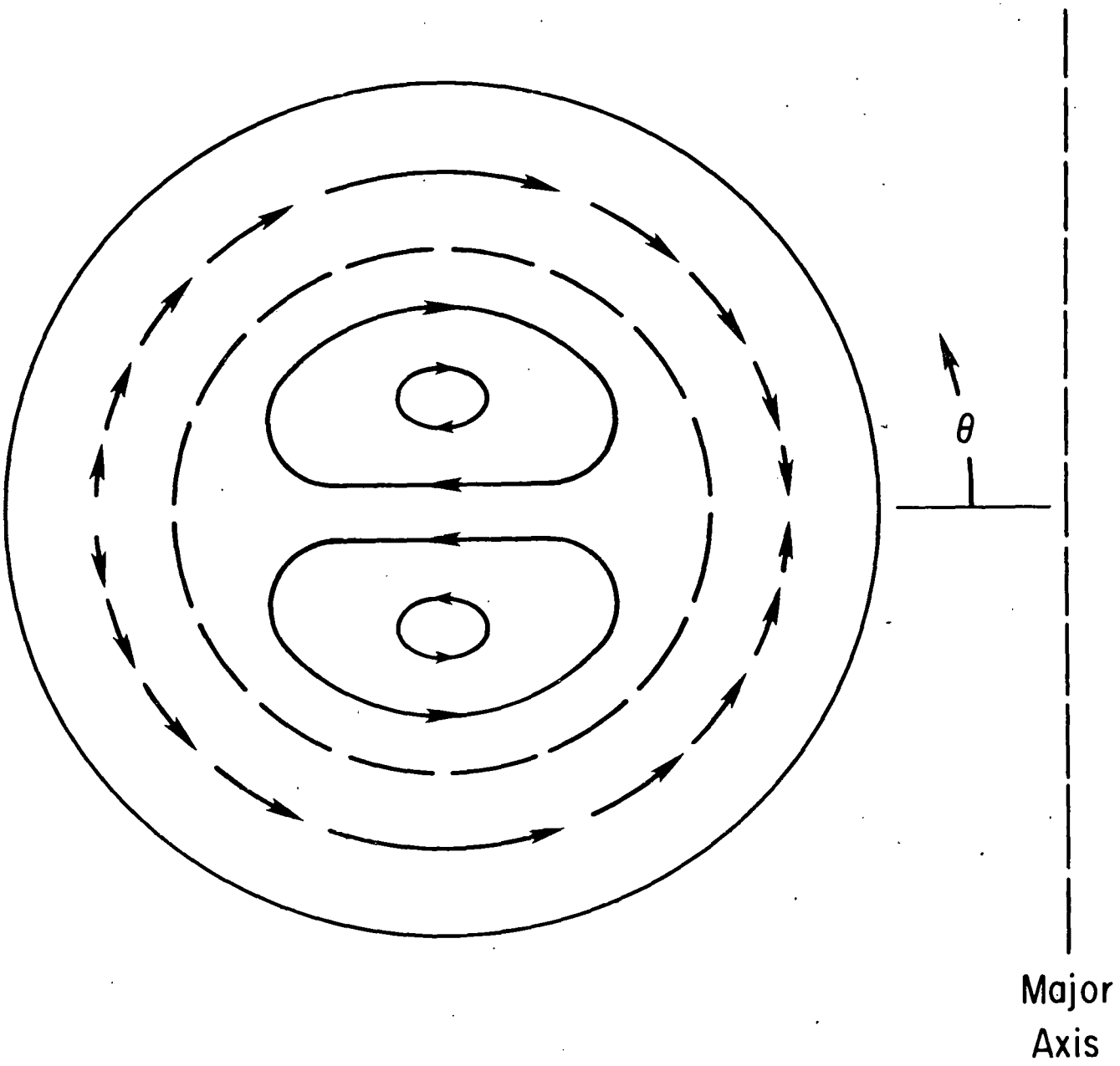

762261

Fig. 6. Inside dotted line: Bulk plasma convective flow, as in Fig. 1(a). Outside dotted line: Subsonic boundary layer flow. Note the matching.

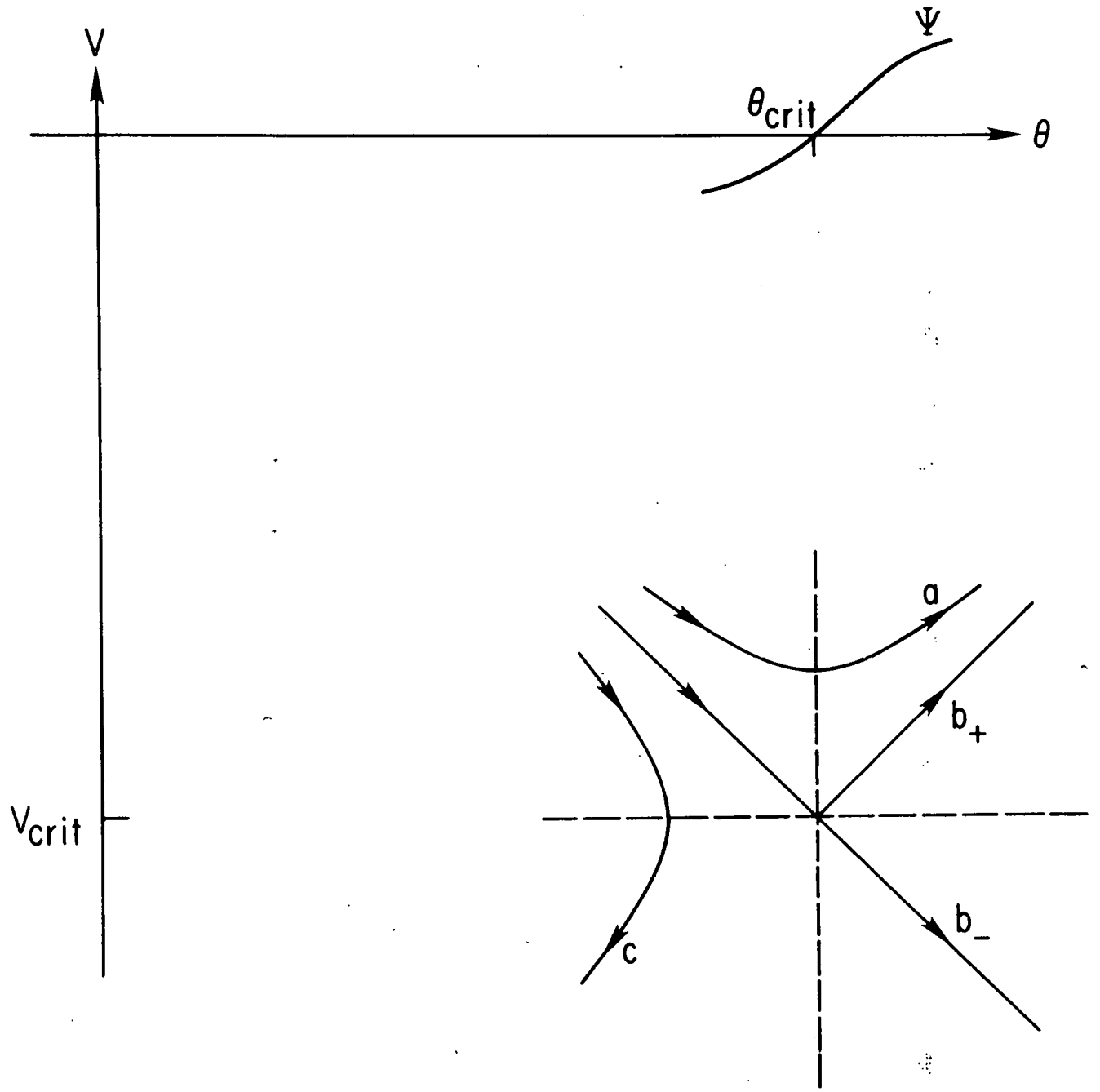

762263

Fig. 7. Possible solutions of Eq. (38): (a) Subsonic solution, $(b)_+$ Just sonic solution, $(b)_-$ Transonic solution, (c) Possible shock solution branch.

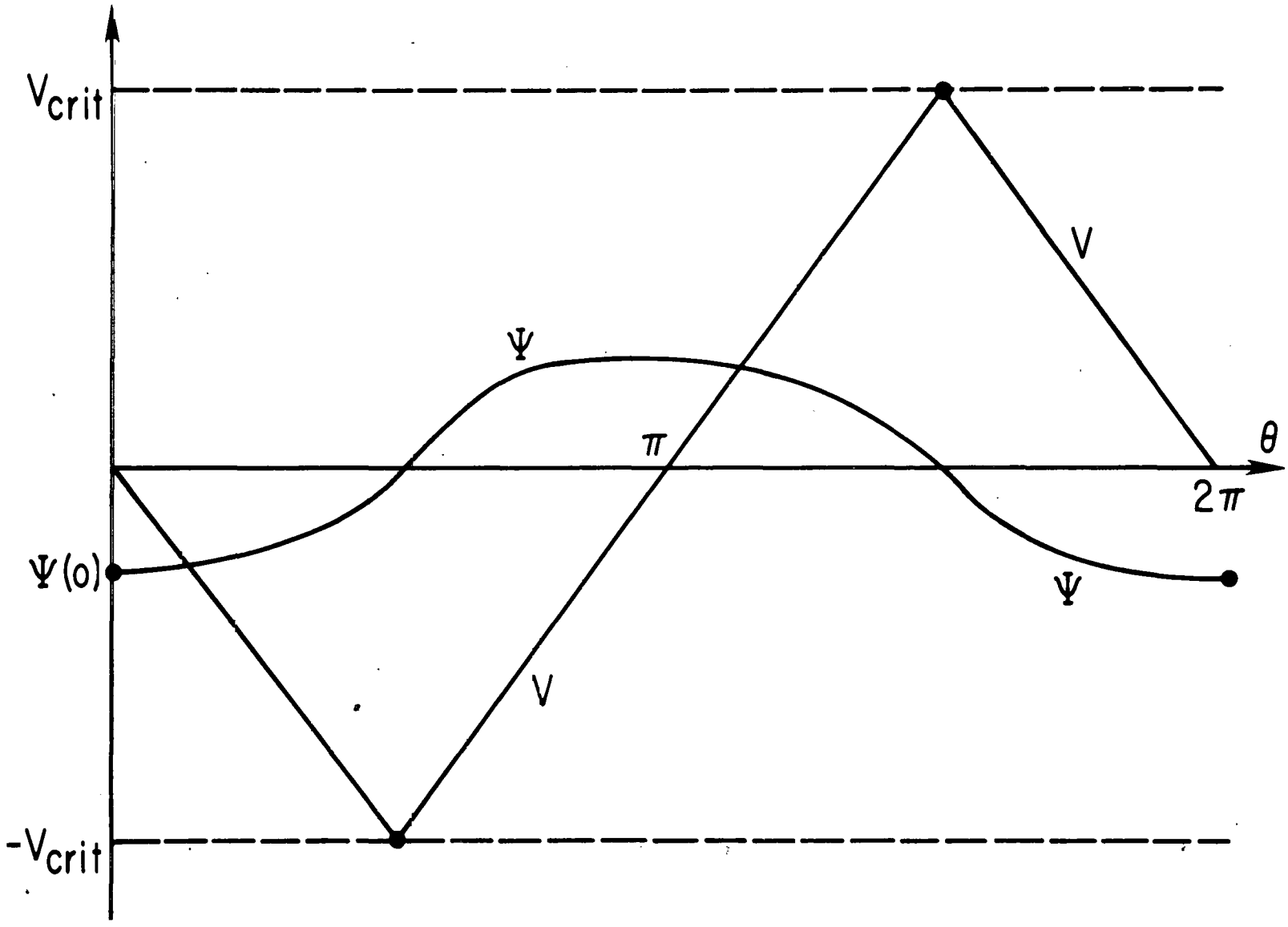

762267

Fig. 8. Just sonic solution for parallel flow (v) and radial flow (ψ).

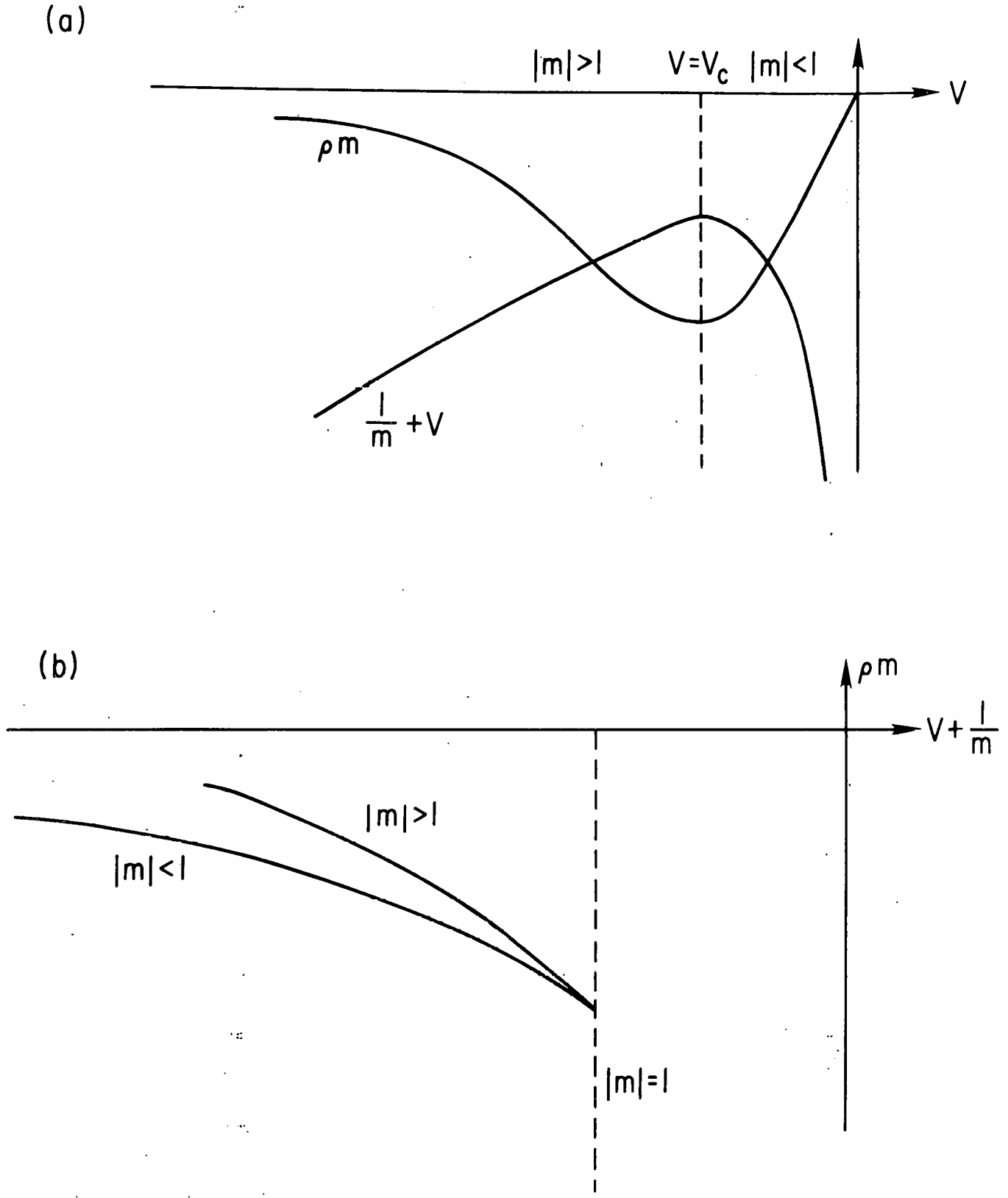

Fig. 9. (a) Mass flux (ρm) and momentum flux (1/m+v) as functions of parallel velocity, v. (b) Fluxes as function of one another.

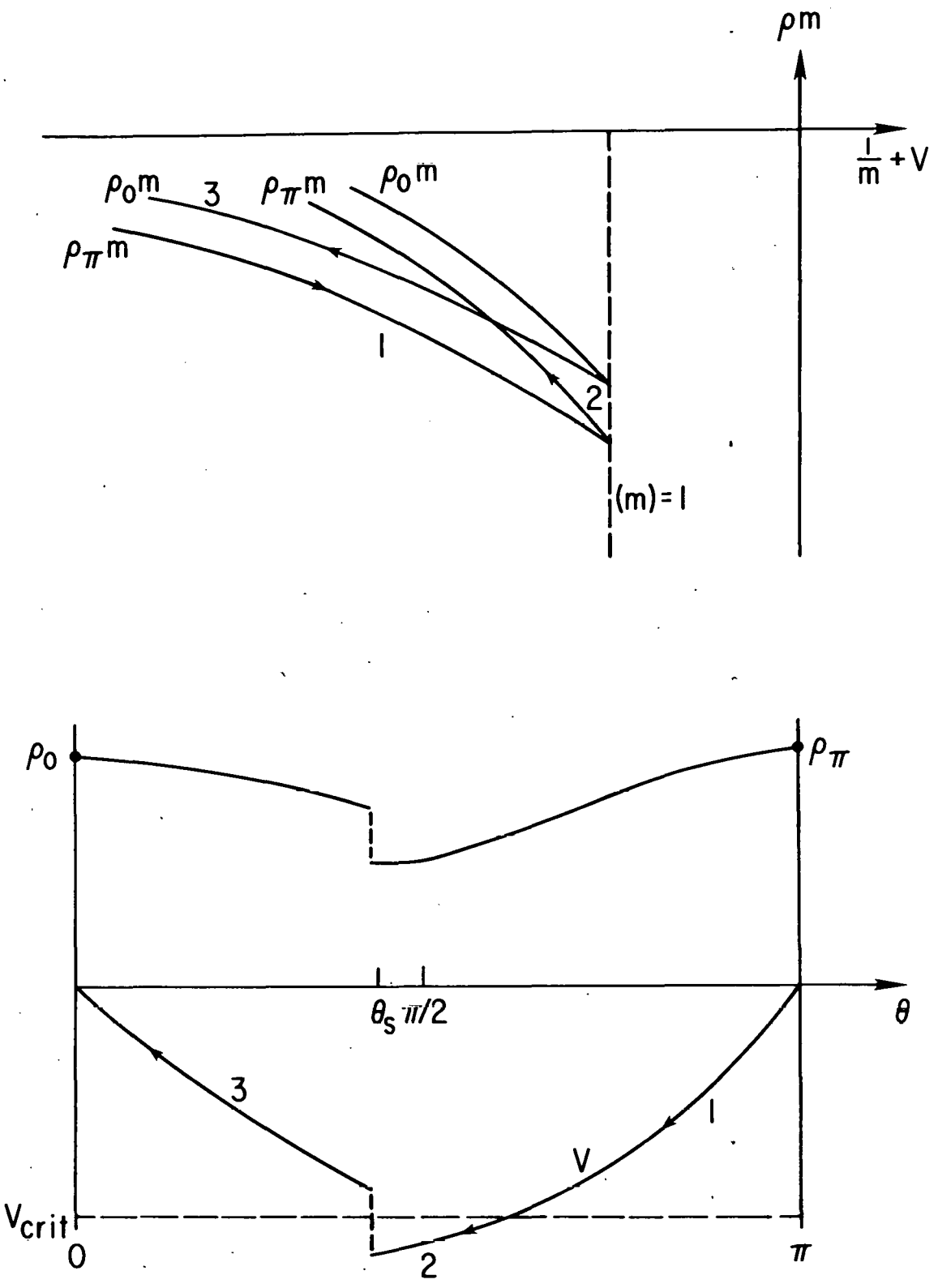

762269

Fig. 10. Flux conserving shock construction. Solution emanates from $\theta = \pi$ along (1). Goes transonic and continues along (2). Shocks back to solution emanating from $\theta = 0$ and returns to $\theta = 0$ along (3).

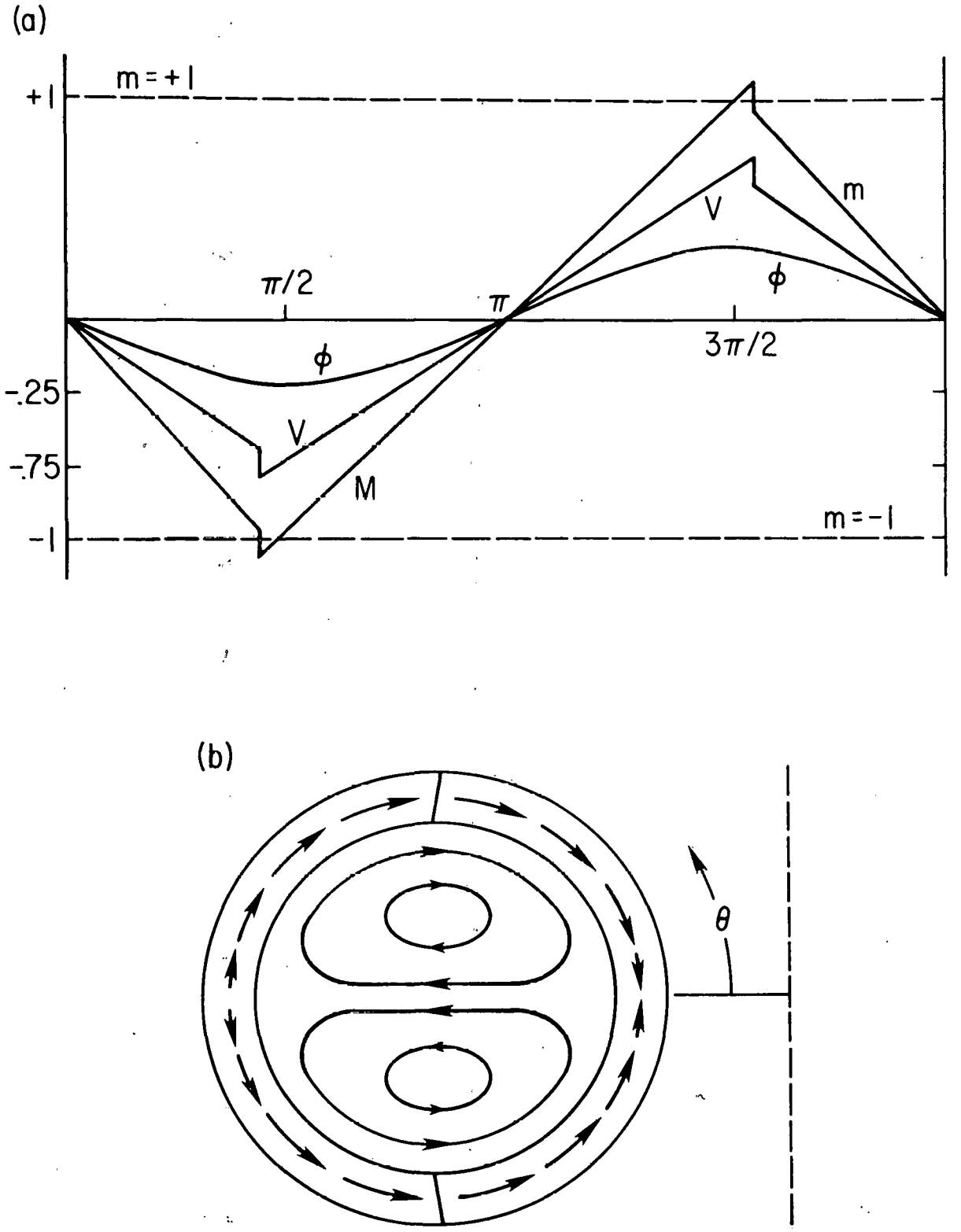

762271

Fig. 11. (a) Shock solutions for parallel flow (v) electric potential (ϕ) and poloidal flow (m). (b) Matching of these boundary layer solutions to bulk plasma convective flow.